Lidar Performance and Calibration Measures for Environmental Mapping

Martin D. Adams
School of Electrical & Electronic Engineering
Nanyang Technological University, Singapore

Abstract

A particular class of sensors often applied to the extraction of environmental information is the lidar (light detection and ranging) system. The aim of this article is to examine the performance limits and sources of systematic and random errors in these sensors at their design and calibration stages and during their general use. A framework, aimed directly at optimising the quality of the output information is given. The design concepts for producing correct range estimates and scanning/sampling rates under all reasonable environmental conditions is derived.

The issue of temporally averaging several range values is also demonstrated and it will be shown that under certain quantified conditions, range variance reduction is possible.

1 Introduction

The correct interpretation of the data produced by any sensor, scanning within indoor environments in the presence of differing surface reflectivities, textures, relative orientations and ranges should begin with an analysis of its hardware design. The sources of electronic noise, non-linear behaviour, signal saturation and even erroneous signals should, at least, be known and understood during the sensor's use or, ideally, minimised at its design stage.

This article has two aims, firstly to pinpoint the critical factors and performance limits in light detection and ranging (*lidar*) sensors which are often used in robot navigation systems [1, 2, 3], and secondly to provide a robust and correct calibration procedure. Section 2 takes an in depth view of the critical design factors in lidar range estimation and section 3 presents the theoretical performance limits, resulting from various noise sources, which can be estimated before lidar electronic construction takes place. Section 4 explores the causes of, and presents remedies for, systematic range errors. The use of the amplitude of the received signal is related to the range variance. Provided both the range estimate and the signal amplitude are available, the ingredients for a theoretically correct range and range variance calibration result. This is the subject of section 5. The speed at which an optical beam can be scanned and hence independent range samples recorded, is the subject of section 6 and finally section 7 explores the possibility of averaging several range estimates, recorded at high speed, for range estimation improvement.

Throughout the article, references will be made to various lidar electronic modules, a detailed explanation of which can be found in [4].

2 Critical Lidar Design Factors

In order to gain an understanding for the systematic and random errors, a review of the physics of reflection and signal reception is necessary. When incident upon an opaque surface, a light ray undergoes both *specular* and *diffuse* reflection simultaneously, and it is the diffuse component which dominates the range estimate for most indoor surfaces, and which is of interest in lidar design [5]. If the transmitter produces an RMS radiant power P_T incident upon a surface at an angle θ relative to the local surface normal (figure 1), the reflected power per steradian, as a function of the angle θ, is $I_R = \frac{P_T \rho \cos\theta}{\pi}$, where ρ is the diffuse reflectivity, which, in general, is a function of the transmission wavelength.

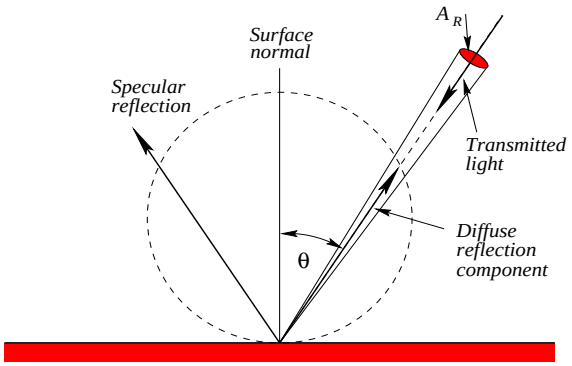

Figure 1: *The variables which affect diffuse reflection.*

If the receiver aperture has an area A_R and is situated a distance r from the illuminated spot (figure 1), then it subtends a solid angle $\alpha = \frac{A_R}{r^2}$. The total power then received is P_R where:

$$P_R = \eta \frac{A_R P_T \rho \cos\theta}{\pi r^2} \qquad (1)$$

where η is the receiver's quantum efficiency. It can be seen from equation 1 that the received power is proportional to $\rho \cos\theta / r^2$. Diffuse reflectance ratios can vary between approximately 0.02 for dark objects and almost 1.0 for white surfaces [5]. As an example, if objects are to be visible to the sensor at incidence angles $0^o < \theta < 80^o$ (i.e. near tangential reflection)

and for ranges $0.2 < r < 15.0$m, the received signal can have a dynamic range of $1.620 \times 10^6 : 1$ or 124 dB[1]. This issue is considered in section 4 where electronic compression circuits will be addressed, to cope with the dynamic range of the received signal.

The received optical power, P_R, induces a proportional current in the photo receiver. Hence the design specifications for a lidar[2] are based upon the *minimum photo detector current* which can be faithfully detected amidst all other current noise sources, and its *dynamic range*, which must not exceed the linear operating region of the ensuing electronics.

3 Performance Limits — Noise

To ensure that the above criterion can be met, the sources of noise and their possible reduction within the sensor's receiver must be addressed. The total noise current is primarily caused by four effects:

1. A *shot noise* component as a result of the photo receiver's *dark current* $\hat{i}_{dark-shot}$.
2. A noise current source due to *avalanche multiplication* (if an avalanche photo-diode (APD) is used) $\hat{i}_{apd}$.
3. A *shot noise* component due to back ground illumination $\hat{i}_{bg-shot}$.
4. A *shot noise* component due to the induced signal current itself $\hat{i}_{rec-shot}$.

The total RMS noise current is then:

$$\hat{i}_{tot\ (RMS)} = \sqrt{\hat{i}^2_{dark-shot} + \hat{i}^2_{apd} + \hat{i}^2_{bg-shot} + \hat{i}^2_{rec-shot}}$$

It now remains to determine the minimum signal current amplitude which needs to be detected and selected from the APD, and ensure that this is much larger than the RMS total noise current defined in the above equation. This gives rise to a further question: "How high does the signal to noise (SNR) ratio need to be for reliable range estimation?" By estimating the nature of the probability distribution of the phase (and hence range) estimate, Brownlow derived an expression for the probability that the error in a given range measurement is less than a predefined value [6]. As would be expected, this probability value increases dramatically with increasing SNR, and for a 10 MHz modulation index (as used in this design), it can be shown that to achieve 99% confidence that all range measurements are within a tolerance of 1% of the maximum range, a minimum SNR of 30 dB is necessary [4].

Substituting each individual noise current estimate into the above equation gives the result:

$$\hat{i}_{tot\ (RMS)} = \sqrt{KB + 2qI_{rec}B} \qquad (2)$$

where K is the mean square noise current per Hz due to the dark current, back ground illumination and avalanche multiplication. For a SNR of 30dB,

$$I_{rec} \geq 32\sqrt{KB + 2qI_{rec}B}. \qquad (3)$$

From equations 2 and 3 it is therefore necessary to proceed with the receiver analysis by:

1. adjusting the necessary design parameters, or sensor specifications, such that the minimum current to be detected I_{rec} obeys inequality 3.
2. constructing a low bandwidth receiver capable of selecting this signal (minimising B) [6].

4 Error – Causes & Remedies

4.1 Systematic Range Errors

In most lidar systems, systematic range errors are reported to be of greater concern than random errors [2, 7]. This is clearly demonstrated in figure 2. The

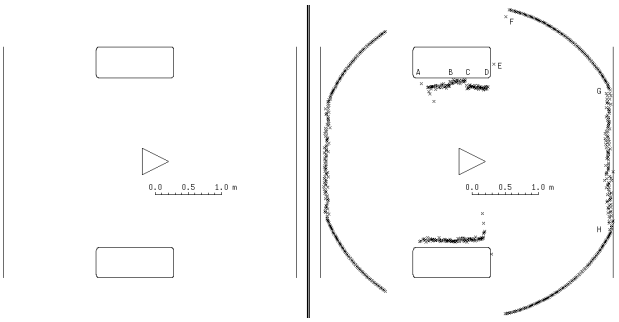

Figure 2: *A single 360° scan taken in a laboratory. Only the unadjusted range data is shown, and each data point is represented as a cross. Curved regions such as FG correspond to out of range readings.*

left plan shows a simple line model of the environment surrounding the sensor (located at the centre of the triangle). The right scan was recorded from a commercially available AMCW lidar sensor, measuring to 2.5m [3]. Due to the differing amplitudes of the received signals from each part of the upper pillar (the reflectivities of the surfaces were different between AB, BC and CD), a clear systematic range error has occurred. This indicates the necessity for controlling the amplitude of the received signal, to ensure linear range estimation throughout the entire specified dynamic range of the received signal. It can also be seen near the upper right corner of the lower pillar that range readings lower in value to those from the pillar edge itself are recorded. This is due to the considerably weakened signal which results from the split beam at the corner, caused by multiple path effects [8, 9]. It is at these points where the signal strength is extremely weak that any "ghost" or internal leakage[3]

[1] These were the design specifications for the construction of the lidar used in this article.

[2] irrespective of the measurement principle (amplitude modulated continuous wave (AMCW), time of flight (TOF) etc.)

[3] This results from either direct electronic cross talk or an optical path which exists directly between the transmitter and

path corrupts the range estimate.

4.1.1 Dynamic Range Compression

The gain of the receiver stage should be set such that the largest received signal, with which the sensor is to function under its design specifications, is linearly amplified meaning that no unwanted phase shifts are produced due to saturation of its output signal. At the output of this stage, weak signals can still be too small for use in the mixing and phase discrimination stages of the sensor. *Automatic gain control* (AGC) systems provide an unsatisfactory solution since at low signal amplitudes, the AGC circuit is controlled by noise [10, 3]. Techniques used in radar technology include the application of log-limiting amplifiers which guarantee minimal phase shift between input and output over a very large input dynamic range [9]. This form of amplitude control is demonstrated in the two graphs of figure 3 where it can be seen that weak signals are linearly amplified by the cascade of amplifiers, whereas strong signals are effectively clipped, whilst preserving the phase information.

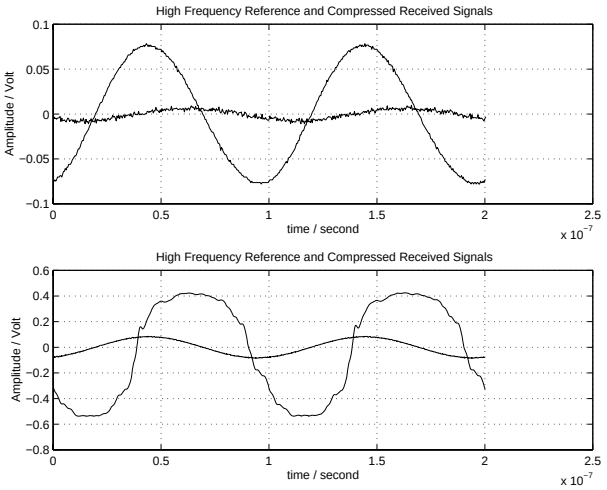

Figure 3: *Weak received signal (top) and strong received signal (bottom), after amplification by the log-limiting amplifiers. The reference signal is also shown in each case (the larger sine wave in the upper graph).*

4.2 Random Error Quantification

For lidar calibration purposes, the *propagation* of the noise sources, given in section 3, must be quantified. The photo-diode produces a time varying current at the frequency of the modulating signal and a noise current $\hat{i}_{tot\,(RMS)}$ (equation 2). The noise in the amplitude of the received signal is not directly of interest in AMCW measurement systems, since the range estimate arises from the relative phase between the zero crossings on the ωt axis of the received and transmitted signals. The resulting range variance σ_r^2, varies with the received signal amplitude V_r as [4, 3]:

$$\sigma_r^2 \approx \left(\frac{\lambda\sigma_n}{4\pi}\right)^2 \left(\frac{1}{V_r}\right)^2 + \sigma_e^2 \qquad (4)$$

where λ is the modulation wavelength, σ_n^2 is the combined constant variance of the electronic noise sources (quantified in section 3), and σ_e^2 is the additive electronic noise variance which results *after* the amplification, mixing and phase comparison stages.

5 Correct Calibration

This section considers the necessary procedures for determining the *three* relationships necessary to provide a full calibration of an AMCW lidar, namely: **Calibration 1:** the output range voltage versus actual range; **Calibration 2:** the internally induced electronic phase shift versus returned signal strength and **Calibration 3:** the range variance versus returned signal strength.

Calibration 1: To eliminate the varying effect of calibration 2, it is *essential* that when initially calibrating voltage versus range, the returned signal strength is held constant, by using, for example, different coloured targets. The left graph in figure 4 shows an initial calibration of sensor output voltage versus actual sensor to target distance. This graph

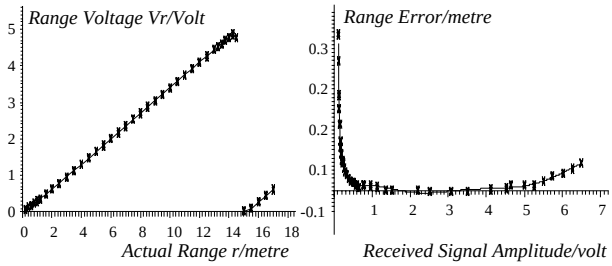

Figure 4: *Calibration curves* **1** *and* **2**.

offers a correct calibration for a target at any range from the sensor, provided it returns a constant signal amplitude. This curve will only approach linearity, if optical and electronic leakage between the transmitter and receiver is minimised.

Calibration 2: The data points in the right graph of figure 4 show the error caused by the amplifiers within the receiver circuit relative to the initial calibration in the left graph. It is interesting to note that various combinations of target reflectance; orientation of target normal relative to the emitted light beam, and sensor to target distance will affect the returned signal strength [11, 12]. *Experiment shows that the factors which affect the returned signal strength are irrelevant as far as modelling the sensor is concerned and it is only the returned signal strength itself which is of importance.* An analytical model for the right curve is not necessary here and would provide no *general* insight into the problem, as similar sensors exist which use other circuits before phase detection

receiver. The detection and removal of these points is covered in [4, 2]

[11, 3, 5]. It is essential however, that this calibration is carried out.

Calibration 3: To establish the range variance as a function of the received signal amplitude, 10,000 independent range measurements were made of fixed targets with the sensor stationary. This must be carried out, whilst adhering to the sampling time constraint, to be explained in section 7. The histograms in figure 5 have horizontal axes showing the measured range r, produced from the left calibration curve of figure 4, and vertical axes showing the number density. Note that the distributions are normalised, since

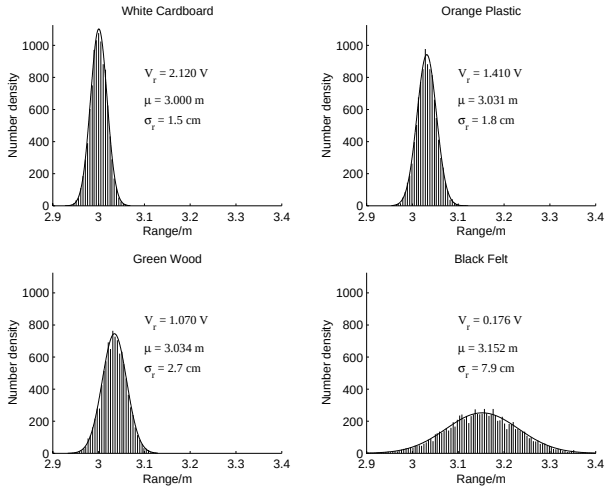

Figure 5: *Histograms showing the effect of different coloured targets at a given range. The signal strength values V_r, sample means μ and range standard deviations σ_r are shown with each graph. The continuous curves show calculated Gaussian distributions with the same mean and variance as the discrete data.*

the sum of the heights of all the range measurements is constant (10,000 in this case). All of the histograms in figure 5 were produced from different targets at a fixed range (3.0 metres) from the sensor. As expected, different signal strength values correspond to different variances within the range values. Note that the distributions are approximately Gaussian[4]. Figure 5 also shows the changes in the sample mean of the ranges for different signal strengths, which must be compensated for by calibration 2. These results can be used to determine the unknown constants σ_n and σ_e in equation 4 and hence the numerical relationship between σ_r^2 and V_r[5]. It should be noted that the range variance cannot increase without limit, since the phase measurement of an AMCW range finder is defined modulo 2π. Therefore the range is defined modulo $\lambda/2$ which is the ambiguity interval of an AMCW lidar (left graph, figure 4).

The use of calibration 3 is demonstrated in figure 6 where the upper scan shows the amplitude of the received signal as a function of the scanning angle, and the lower scan shows the standard deviation in range. The lower scan shows lines of length $2\sigma_r$, calculated from the received amplitude in the upper scan and equation 4, centred on the actual range estimates themselves. For Gaussian range distributions, as suggested in figure 5, the actual range value must lie within the line segments of figure 6, with a probability of 95 % [15].

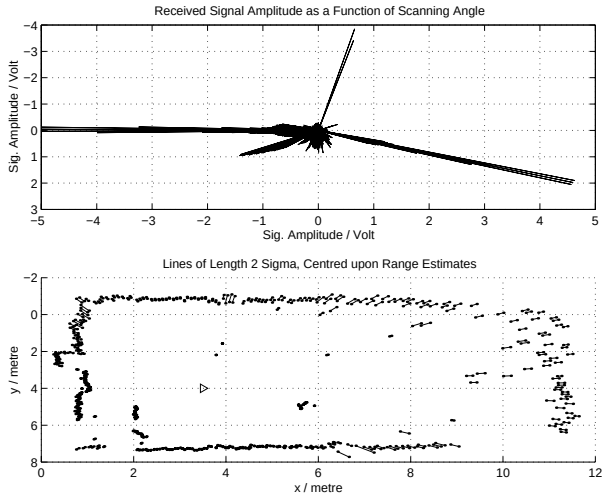

Figure 6: *Signal amplitude (top) and lines of length $2\sigma_r$ centred on the range estimates (bottom).The triangle shows the position of the mobile robot.*

6 Possible Scanning Speed

The range processing of the transmitted and received signals, needs to estimate their relative phase. A reliable tool for producing square waves locked in phase to almost any noisy periodic input signal is the *phase-locked loop* (PLL). To ensure that the PLL is able to track the dynamic phase variations of the received signal, as the sensor scans, it is necessary to analyse its components, namely the low pass filter used in conjunction with the phase detector and the voltage controlled oscillator (VCO). A simple schematic block diagram of the PLL is shown in figure 7. The stability of the control loop is improved if a 'lead-lag' low pass filter is used meaning that $G(s)$ in figure 7 has the form:

$$G(s) = \frac{1 + sT_2}{1 + s(T_1 + T_2)} \tag{5}$$

If the gain of the phase comparator is K_p and that of the VCO is K_{vco}/s, the overall closed loop transfer function between the phase of the input sinusoid ϕ_{in}

[4] For very weak received signals, it can be shown that the distributions are Rayleigh in form [13, 4].

[5] Note that a TOF lidar will also produce randomly distributed range estimates but the analysis should be based upon the finite rise time of the received pulse as a function of the received signal intensity. In general TOF lidars suffer more than their AMCW counterparts if the received signal is weak as false detection, or no detection at all can result. An AMCW lidar will produce a noisy but consistent range estimate, assuming correct calibration [14].

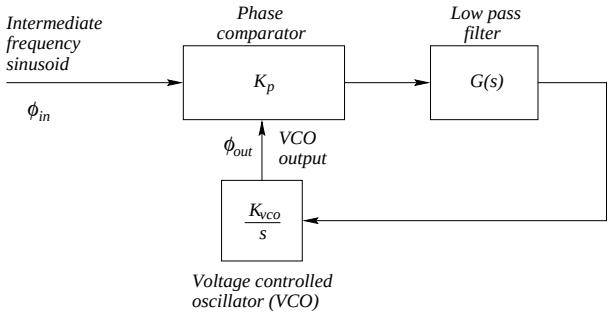

Figure 7: *Block diagram of the phase locked loop.*

and the output square wave ϕ_{out} is given by:

$$\frac{\phi_{out}}{\phi_{in}} = \frac{K_{vco}K_p(1+sT_2)}{s^2(T_1+T_2)+s(1+T_2K_{vco}K_p)+K_{vco}K_p} \quad (6)$$

which produces a classical second order response (with damping factor ζ and natural frequency ω_n) to changes in the input phase, caused by range changes. With knowledge of the possible speed at which the input phase can change with respect to time and the desired settling time for the locally produced VCO output square wave, values for ζ and ω_n can be calculated and implemented by choosing the correct components in the lead-lag low pass filter. The highest frequency changes in range which need to be recorded correspond to a change of maximum range (15m in this case) divided by the time necessary for the scanning mirror to rotate through the effective beam width of the light spot. Within this time interval, it is necessary that all transient effects of the transfer function of equation 6 have reached an acceptable level. Brownlow defined this "acceptable level" as the time period $t = 3\pi/\omega_n$ after which any overshoot has reduced to less than 1cm range error [6].

The frequency lock-in detection capability of the PLL is demonstrated in figure 8 where the top graph shows the received (low amplitude, noisy wave) and reference signals from a target at 7.0 metres. The lower graph shows the square wave outputs from the two VCOs running on separate PLLs. The reference 'square' wave has been shifted vertically by 2.0 volts so that both wave forms can be clearly seen. The subsequent processing necessary to produce an analogue output proportional to range, simply requires a suitable phase detection circuit with both of these square waves as inputs. To demonstrate the effect of the received noise, figure 8 shows the results recorded from the VCO outputs at 5 different time intervals, these being superimposed upon each other in the lower graph. It can be seen that the time axis crossing of the received signal is ill defined (large phase noise) due to its low SNR. Hence ultimately, range uncertainty results.

A "good" reflector placed 7 m away from the sensor, was used for the same experiment in figure 9. This time, the larger signal is the received signal in the upper graph, and once again the received signal's VCO output was recorded at 5 instants in time relative to the reference VCO signal. It can be seen that the time axis crossings are more clearly defined and the phase noise is greatly reduced.

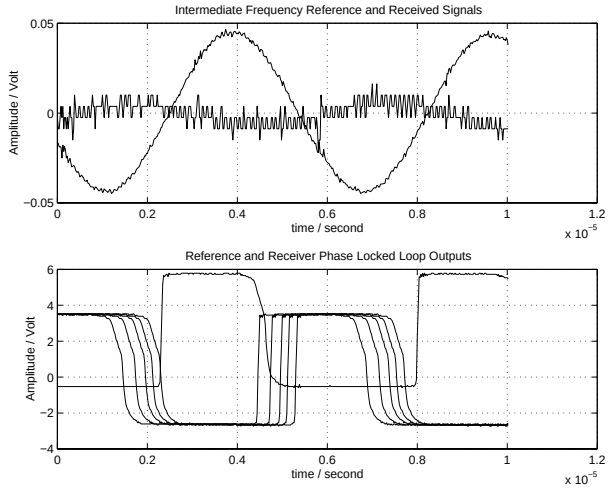

Figure 8: *Reduced frequency reference and received signals (top) and their corresponding VCO outputs (bottom) for a weakly reflecting target at 7.0m.*

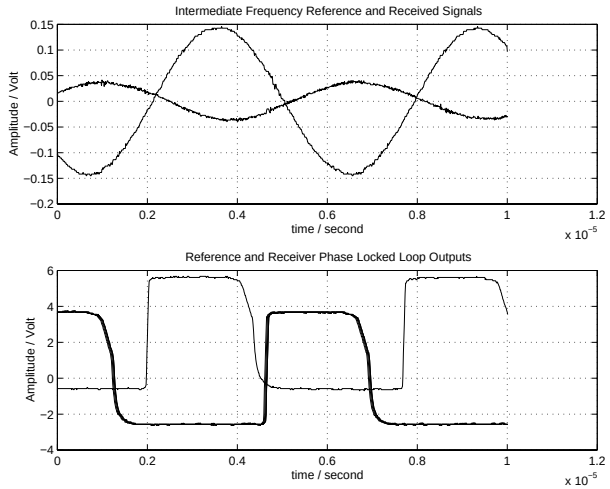

Figure 9: *Reduced frequency reference and received signals (top) and their corresponding VCO outputs (bottom) for a reflective target at 7.0.*

7 Averaging of Range Data

Section 4.2 quantified the range variance of a single range sample. It can be shown that if the sampling time interval ΔT, between range measurements is much less than the sensor's output filter time constant T_f (high correlation between successive samples) then the standard deviation $\bar{\sigma}_r$ of the average of n samples is given by [10]:

$$\bar{\sigma}_r = \frac{\sigma_r}{\sqrt{n_{eff}}} \quad (7)$$

where, for a single pole filter, if $n\Delta T << T_f$, then $n_{eff} \approx 1$ [5]. If however:

$$n\Delta T >> T_f \tag{8}$$

$n_{eff} \approx (n\Delta T/2T_f)$. Note that this result is only true for $\Delta T << T_f$ and in any case, n_{eff} can never be larger than n, the number of samples recorded. Hence if a target can be sampled such that the product $n\Delta T$ is greater than $2T_f$ an improvement in the confidence in the range estimate results, since $\bar{\sigma}_r$ is reduced. The important point to note here is that due to the finite size of the optical transmitter footprint, this averaging technique can reduce the noise in the range image *without* degrading its resolution [4].

The above criterion was used to reduce the range error in figure 10 where two 3D scans are shown after systematic range error compensation (section 5). The

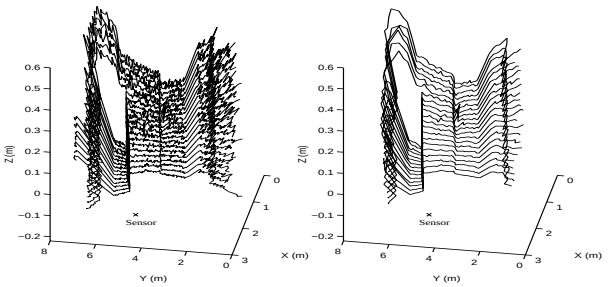

Figure 10: *Range data showing the corner of a room from a single 3D scan. The left scan shows all recorded data points from the section under consideration, and the right scan shows only one sample averaged from every 4 range points.*

left scan shows a corner of an environment containing cupboards and a chest of drawers, each sample taken every 0.5^o of sensor head rotation. Every 4 of these were averaged to form a single data point in the right range map. The improvement in the range variance is evident. In this case $4\Delta T = 2.8$ms, which is about ten times larger than T_f, corresponding to a filter cut off frequency of 3.5kHz.

8 Summary

The physics behind environmental reflection and signal reception provides a solid foundation for the critical design factors in lidar design. A minimum detectable receiver photo-current was derived as a function of various parameters, including noise, attributed primarily to the receiver electronics, which oppose its reliable detection.

A solution for minimising systematic range distortion, using amplitude compression was presented, along with an exact calibration procedure for removing systematic range errors, and quantifying the range variance with each range sample. In general it is crucial to note that the *naive determination of the output range voltage from AMCW or TOF lidars as a function of the sensor to target range, in general provides a false calibration.*

The speed at which independent range data can be recorded, and hence the possible scanning speed, can be quantified in terms of the phase detection electronics in an AMCW lidar. Further noise reduction in the range data results if several points are averaged under the quantified temporal constraints in section 7.

References

[1] Sick Optic Electronic. *Sick Aktuell 2/97.* Erwin Sick AG, CH - 6370 Stans, Switzerland., 1997.

[2] M. Hebert and E. Krotkov. 3-D measurements from imaging laser radars: How good are they? In *Int. Conf. Intelligent Robots and Systems*, pages 359–364, 1991.

[3] G. L. Miller and E. R. Wagner. An Optical Rangefinder for Autonomous Robot Cart Navigation. Technical report, A.T&T. Bell Laboratories, Princeton NJ., 1987.

[4] Martin D. Adams. *Sensor Modelling, Design and Data Processing for Autonomous Navigation.* World Scientific, 1999.

[5] D. Nitzan, A. E. Brain, and R. O. Duda. The measurement and use of registered reflectance data in scene analysis. In *Proc. IEEE.*, pages 206–220, vol. 65, 1977.

[6] M. J. Brownlow. *A Time of Flight Optical Range Sensor for Mobile Robot Navigation.* PhD thesis, University of Oxford, United Kingdom., 1993.

[7] J. Borenstein, H. R. Everett, and L. Feng. *Navigating Mobile Robots: Sensors and Techniques.* A. K. Peters, Ltd., Wellesley, MA, 1995.

[8] M. D. Adams and P. J. Probert. The interpretation of phase and intensity data from amcw light detection sensors for reliable ranging. *Int. J. Robotics Research*, 15(5):441–458, 1996.

[9] Merrill I. Skolnik. *Introduction to Radar Systems.* McGraw-Hill, 1962.

[10] M. D. Adams. *Optical Range Data Analysis for Stable Target Pursuit in Mobile Robotics.* PhD thesis, University of Oxford, United Kingdom., 1992.

[11] G. Allègre and H. Clergeot. A Two Dimensional Laser Rangefinder for Robot Vision and Autonomy. In *Int. Conf. Intelligent Robots and Systems*, pages 371–376, 1991.

[12] T. Okada and U. Rembold. Proximity sensor using a spiral-shaped light emitting mechanism. *IEEE J. Robotics and Automation*, 7(6), 1991.

[13] Connor F. R. *Noise.* London: Edward Arnold, 1982.

[14] P. Vuylsteke, C.B. Price, and A. Oosterlinck. Image sensors for real-time 3D acquisition, part 1. In T.C. Henderson, editor, *Traditional and Non-Traditional Robotic Sensors*, pages 187–210. Springer Verlag, 1990.

[15] Erwin Kreysig. *Advanced Engineering Mathematics.* John Wiley & Sons, 5th edition, 1983.